

# Unraveling the Turn-On Limitation of Quantum-Dot Electroluminescence via a Stepwise-Increasing Voltage Measurement

Xiaoxiang Zhu<sup>ID</sup>, Yuechao Wang, and Wenyu Ji<sup>ID\*</sup>

Key Lab of Physics and Technology for Advanced Batteries (Ministry of Education), Department of Physics, Jilin University, Changchun, 130023, China



(Received 21 October 2022; revised 5 January 2023; accepted 18 January 2023; published 3 February 2023)

Whether the electroluminescence turn-on of quantum-dot light-emitting diodes (QLEDs) is determined by electrons or holes has long been controversial. Given that the charge-carrier trapping or/and capturing processes affect the current measured through an organic semiconductor film, then the long-lived trap information can be extracted by measuring the current through the film with a periodic stepwise-increasing voltage. We develop easy-to-operate technology to detect the long-lifetime traps in the organic small-molecule materials and demonstrate that the turn-on behavior of the QLEDs is determined by the hole injection. Moreover, it is verified that the long-lived hole traps are also responsible for the luminance overshoot behavior for the device driven by a constant current. We believe this characterization technology can provide a significant platform to deeply understand the properties of both materials and photoelectronic devices.

DOI: 10.1103/PhysRevApplied.19.024010

## I. INTRODUCTION

Quantum-dot light-emitting diodes (QLEDs) have attracted considerable attention due to their unique photoelectronic properties [1–4]. The performance of QLEDs has made many advances in recent years, with external quantum efficiency reaching over 20% [5,6]. However, the working mechanisms of QLEDs are yet to be understood, such as electroluminescence (EL) turn-on behavior [7,8], the positive aging effect [9,10], the origin of degradation [11,12], etc. Multidisciplinary efforts are needed to reveal the underlying physical mechanisms. The defects in the functional layers constructing the devices play crucial roles in the EL processes of QLEDs. However, there are few reports on this problem.

Defects widely exist in semiconductor materials, and their study deserves great effort due to the various significant influences on the properties of semiconductors and photoelectronic devices [13–16]. In some cases, the defects play a positive role in the photoelectronic properties of semiconductor materials. For instance, charge carriers are mainly transported through the defect states in ZnO and SnO<sub>2</sub> nanocrystal solids by Mott variable-range hopping processes [17,18]. Defect states can also become luminescent centers in AgInS<sub>2</sub> and CuInS<sub>2</sub> quantum dots (QDs) [19,20]. However, in most cases, defects deteriorate the properties of semiconductor films [13,14,21]. The carrier-trapping effect induced by defects decreases the free-carrier concentration, reducing the carrier mobility

[21–24]. Meanwhile, these defect states could also result in exciton quenching, thus reducing the efficiency of photoelectronic devices [14,25,26]. Therefore, it is urgent to gain information about defects and uncover their influence on EL devices.

Various techniques have been proposed so far to detect defects. Space-charge-limited current (SCLC) can estimate the density of traps ( $N_T$ ) using trap-filled limit voltages from the current-density–voltage ( $J$ - $V$ ) curve, which requires unipolar injection, Ohmic contact, and *a priori* assumptions on the energetic profile of traps [27–31]. The capacitance-frequency ( $C$ - $f$ ) properties obtained by impedance spectroscopy are also commonly used to characterize trap density and energy distributions [32–34], which, however, are disturbed by the accumulated charge carriers at interfaces within the devices. Deep-level transient spectroscopy offers a high sensitivity, by which the information of the defects ( $N_T$ , the activation energy  $E_a$ , the capture cross section  $\sigma_T$ ) can be obtained by transient signals (such as voltage, capacitance, current, and charge) at different temperatures [35–37]. However, these methods focus only on the defect information itself, and the influence of defects on the EL devices cannot be obtained *in situ*.

In this work, we develop an easy-to-operate and low-cost technology to characterize the long-lived traps in the organic semiconductor films, which is achieved through recording the current by a periodic stepwise-increasing voltage (CPSIV). This method is based on the physical mechanism by which the charge-carrier trapping and/or capturing processes can induce localized electric

\*jiwy@jlu.edu.cn

field and scattering effects, hence reducing the conduction current through the films [21–23,38]. Thus, the defect information can be extracted from the current difference between the first and second sweeps using current measurements. The hole-trapping properties of 4,4',4''-tris(N-carbazolyl)-triphenylamine (TCTA) and 2,2'-bis(4-(carbazol-9-yl)phenyl)biphenyl (BCBP), commonly used hole-transport materials in both QLEDs and organic LEDs, are measured to validate this CPSIV technology. Moreover, we demonstrate that the luminance overshoot during the initial period during operation lifetime measurements also originates from these deep long-lived defects. Then, the hole-injection voltage is extracted by performing CPSIV measurements, which is demonstrated to determine the EL turn-on of the QLEDs.

## II. METHOD AND EXPERIMENT

As shown in Fig. 1, the defect traps in semiconductors could be simply classified by trap energy ( $E_T$ ) [13]. The shallow traps represent the states whose energy levels are near the valence (or the highest occupied molecular orbital, HOMO) or conduction band (or the lowest unoccupied molecular orbital, LUMO). On the one hand, the multiple trapping and releasing processes of these shallow traps significantly decrease the carrier transport by the conduction or valence band [13,21–23]. On the other hand, in ZnO and SnO<sub>2</sub> nanocrystal polycrystalline films, the charge carriers are transported through the shallow traps with a

hopping mechanism by fast trapping and detrapping processes [17,18]. In contrast, although the deep traps located in the middle of the forbidden bands can also decrease the charge transport (like the shallow traps) by localized electric field and scattering effects, the long trapping and detrapping lifetimes will lead to different electrical changes for the films and devices during sequential sweeps. In other words, the electrical properties will exhibit great dependence on the driving history of the devices. Therefore, it is necessary to uncover the properties of deep long-lived traps in semiconductor films under electrical driving conditions. Our method is specially designed for *in situ* analysis of long-lifetime defect states.

The experimental setup and the equivalent circuit of QLEDs are depicted in Fig. 2(a). From the electrical point of view, the QLED can be modeled by a parallel equivalent circuit consisting of a resistance ( $R_d$ ) and a capacitance ( $C_d$ ), forming the  $RC$  element describing all the functional layers (detailed discussion is given in the Supplemental Material [39]). The  $R_s$  is a series resistor, induced by the electrodes, contacts, and wires. A periodic stepwise-increasing voltage [Fig. 2(b)] is used as the driving source to measure the current across  $R_0$  (device), which shows time-dependent features. The stepwise voltage is described by parameters of amplitude ( $\Delta U$ ), duration ( $\Delta t$ ) of each step, and period ( $T$ ) and total amplitude ( $U_0$ ) of the driving voltage,

$$U(t) = \begin{cases} \Delta U, & 0 < t < \Delta t \\ 2\Delta U, & \Delta t < t < 2\Delta t \\ \vdots \\ -\Delta U, & T - 2\Delta t < t < T - \Delta t \\ 0, & T - \Delta t < t < T \\ \Delta U, & T < t < T + \Delta t \\ \vdots \end{cases} \quad (1)$$

As shown in Fig. 2(c), the transient current response  $i_{tr}(t)$  of the equivalent circuit under the  $n$ th voltage step ( $t_n < t < t_n + \Delta t$ , where  $t_n$  is the starting time of the  $n$ th step) can be written as

$$i_{tr}(t) = U(t) \frac{[(R_0 + R_s) - R_e]}{(R_0 + R_s)^2} + \Delta U \frac{R_e}{(R_0 + R_s)^2} \exp\left(-\frac{t - t_n}{R_e C_d}\right), \quad (2)$$

with

$$R_e = \frac{(R_0 + R_s)R_d}{(R_0 + R_s) + R_d}, \quad (3)$$

where  $C_d$  and  $R_d$  are the equivalent capacitance and resistance of the device. In Eq. (2), the first term represents the device's steady-state current (conduction current)  $i_{SS}(t)$

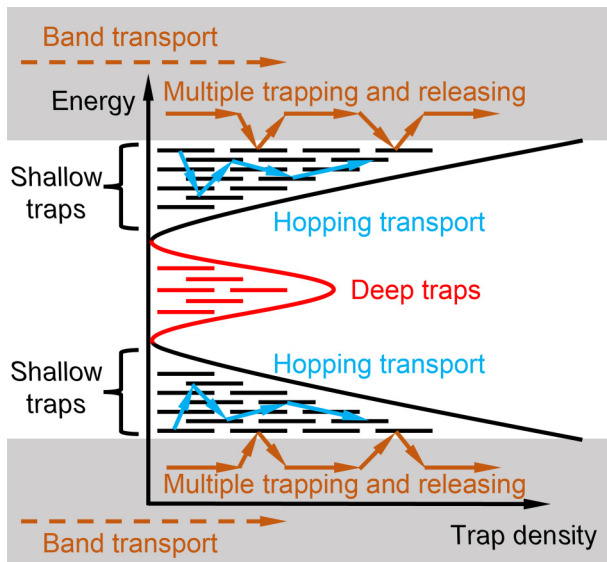


FIG. 1. Schematic trap distribution in semiconductors: shallow traps (black) and deep traps (red) in the band gap. Arrows represent different transport mechanisms: band transport (brown dashed line), multiple trap and release processes (brown solid line), and hopping transport between localized states (blue).

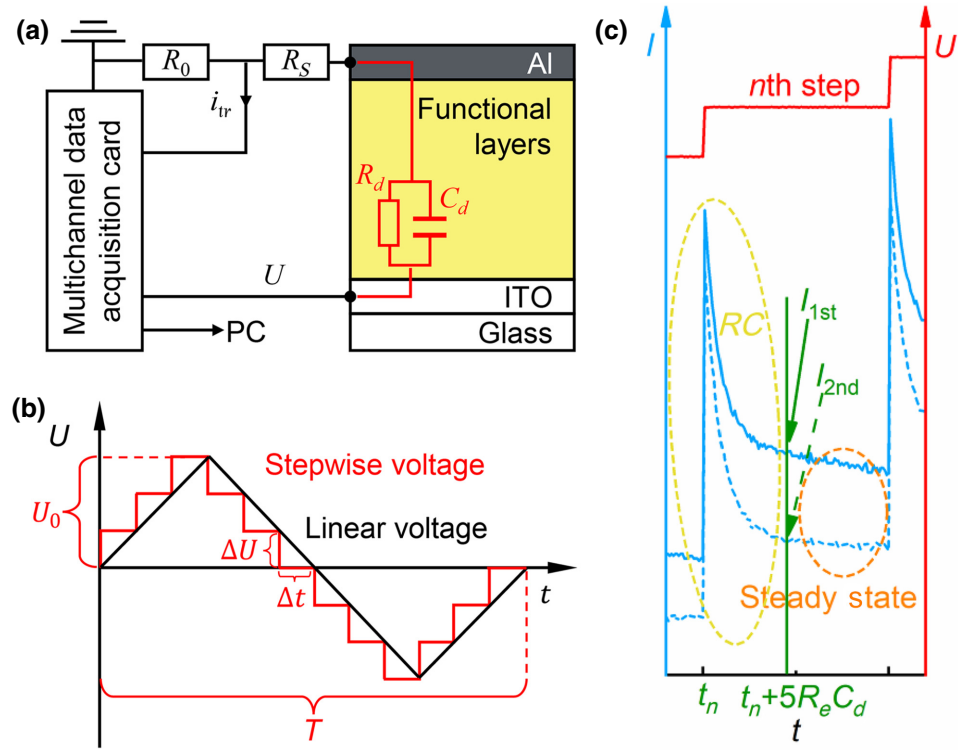


FIG. 2. (a) Measurement setup for the CPSIV. The red lines represent the equivalent circuit of the device. (b) Stepwise voltage (red line) and triangle wave (black line) driving modes. (c) Current response (blue solid and dashed lines) of TCTA-based QLED driven under  $n$ th voltage step (red) of two continuous periods. It involves  $RC$  (yellow ellipse) and steady-state (orange ellipse) components.

and the second term describes the  $RC$  transient current response (displacement current)  $i_{RC}(t)$  under the  $n$ th voltage step. The declining voltage step (from  $0.25T$  to  $0.5T$ ) is used to perform the reverse sweep. The negative voltage step during  $0.5T$  to  $T$  is applied to the device to release or extract the charges in shallow traps.

For the films or devices, where trapping and detrapping processes occur on timescales of hundreds of microseconds or even seconds, the current  $I_{1\text{st}}$  (including  $i_{RC}$  and  $i_{SS}$ ) during the first sweep will be much greater than that obtained during the second sweep,  $I_{2\text{nd}}$ , as shown in Fig. 2(c). In principle, when  $t - t_n = 5R_e C_d$ ,  $i_{RC}(5R_e C_d)$  drops to 0.67% of its maximum value, according to Eq. (2), and the  $i_{\text{tr}}$  ( $5R_e C_d$ ) is close to the steady-state current  $i_{SS}$ . Nevertheless, a reliable steady-state current can only be obtained for  $\Delta t$  over  $10R_e C_d$  during the first sweep, as observed in Fig. 2(c). This is because the  $i_{\text{tr}}$  during the first sweep contains the trap-capturing current, which is not involved during the second sweep due to the long detrapping lifetimes of the traps. The scattering effect and localized electric field induced by these trapped carriers during the first sweep further reduce the steady-state current  $i_{SS}$  during the second sweep [21–23,38]. As shown in the Supplemental Material Fig. S2 [39], the current difference between the first and second sweeps dramatically decreases with increasing  $\Delta t$ , which further

confirms the trap effect on hole transport. Therefore, the current difference of  $i_{\text{tr}}$  at  $t_0 = 5R_e C_d$  between the first and second sweeps can be used to evaluate the charge-trap information.

Compared with the typical triangle voltage used in displacement current measurements [38,40], our proposed CPSIV technology is more suitable to detect the deep traps with long trapping and detrapping lifetimes, such as TCTA and BCBP, whose trapping processes are as long as 45 s and 20 s, respectively (shown in the following text). Moreover, a conduction current  $i_{SS}$  must be avoided or suppressed in the displacement current measurements to evaluate the trapping processes [38]. In contrast, the conduction current  $i_{SS}$  has little effect on the CPSIV measurements, which makes it possible to assess the influence of defects on a working light-emitting diode by *in situ* measurements.

The model devices investigated in this work include a hole-only device (HOD) of indium tin oxide (ITO)/[TCTA ( $\sim 150$  nm) or BCBP ( $\sim 150$  nm)]/MoO<sub>3</sub>( $\sim 8$  nm)/Al ( $\sim 100$  nm), electron-only device (EOD) of ITO/ZnO ( $\sim 40$  nm)/QDs( $\sim 10$  nm)/Al, and the QLEDs of ITO/ZnO/QDs/[TCTA(60 nm) or BCBP(60 nm)]/MoO<sub>3</sub>/Al. The Ohmic contact device with 4,4'-bis(9-carbazolyl)-2,2'-biphenyl (CBP) as interlayer [41] consisting of ITO/poly(3,4-ethylenedioxythiophene) polystyrene sulfonate

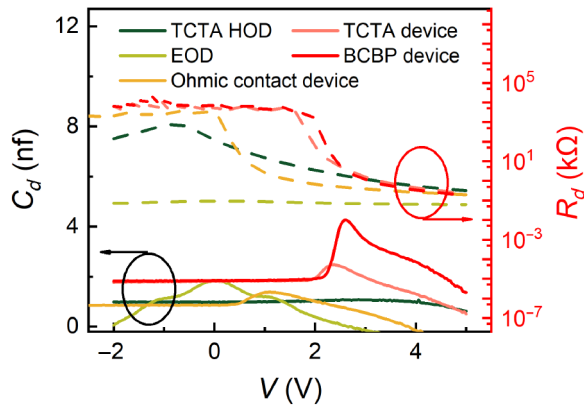


FIG. 3. Capacitance-voltage-resistance curves of different devices.

(PEDOT:PSS) ( $\sim 40$  nm)/TCTA( $\sim 150$  nm)/CBP( $\sim 5$  nm)/MoO<sub>3</sub>/Al is also fabricated to examine the interface effect. The device pixel is  $4\text{ mm}^2$ . Detailed information including the materials, energy levels (Supplemental Material Fig. S3 [39]), device fabrication, and instruments used in this work are described in the Supplemental Material [39]. The energy levels are taken from Refs. [42–44].

The parameters for the periodic stepwise-increasing voltage used in the measurements are fixed as follows:

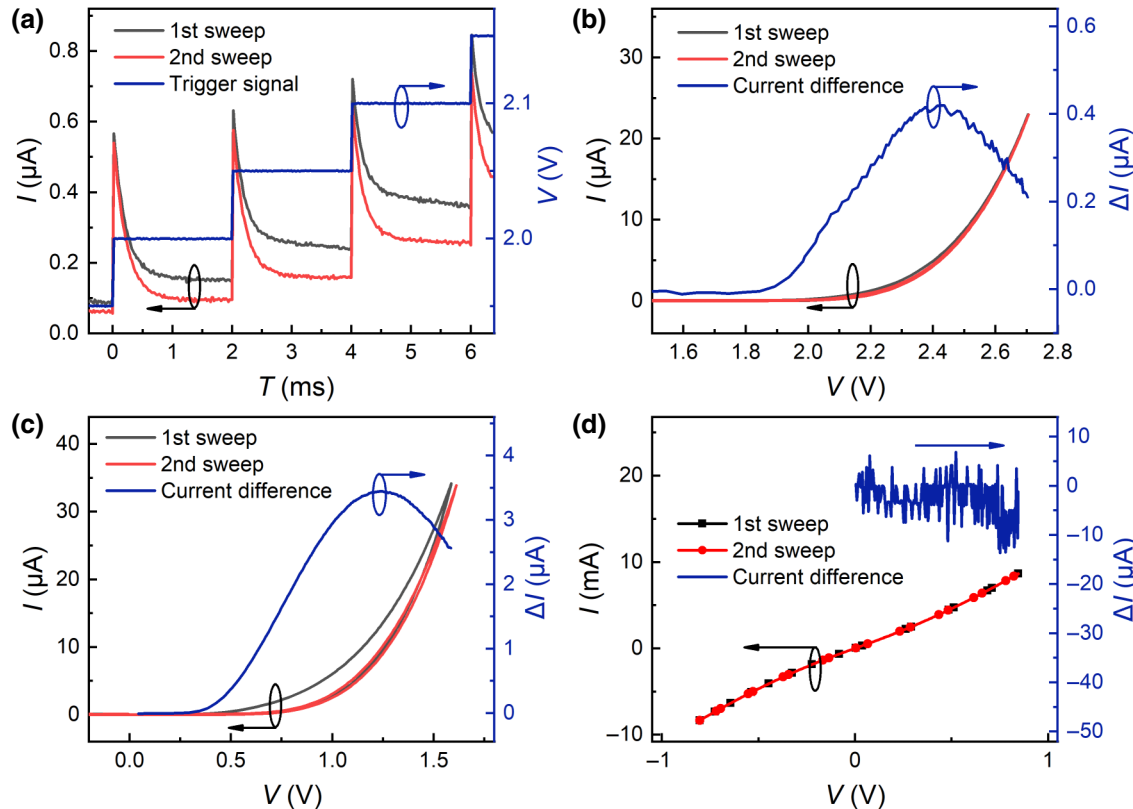


FIG. 4. (a) Time-resolved current of QLED with TCTA under the voltage step. The current of the first and second sweeps and the current difference of these two sweeps in (b) QLED with TCTA, (c) HOD with TCTA, and (d) EOD with QDs.

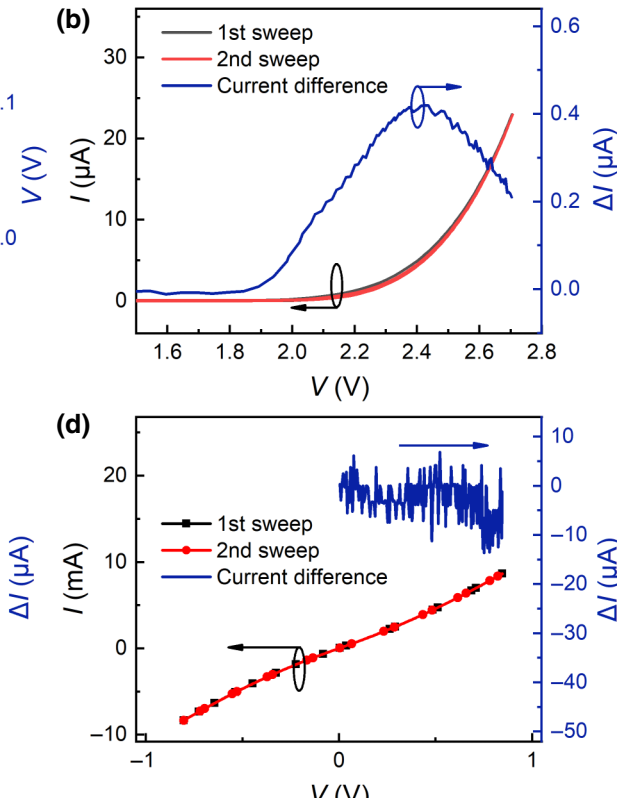
TABLE I. Parameters for the calculation of  $t_0$ .

	$C_d$ (nf)	$R_d$ (kΩ)	$R_0$ (kΩ)	$R_e$ (kΩ)	$t_0 = 5R_e$
TCTA HOD	0.99	791	100	88.8	0.45
EOD	1.84	0.092	1	0.084	0.0008
Ohmic device	0.86	2772	100	96.5	0.40
TCTA device	1.80	5492	100	98.2	0.90
BCBP device	1.83	14 718	100	99.3	0.90
				$C_d$ (ms)	

the voltage step amplitude  $\Delta U = 0.05$  V, the total amplitude  $U = 5.0$  V, and the divider resistor  $R_0 = 100$  kΩ. For the EOD, in order to obtain sufficient time and current resolution, the parameters  $\Delta U = 0.05$  V,  $U = 10.0$  V, and  $R_0 = 1$  kΩ are used. The  $t_0$  of these devices are calculated by the  $C_d$ - $V$ - $R_d$  curves (Fig. 3) and summarized in Table I. Considering the reliability of the experimental results, the voltage step duration of  $\Delta t = 2$  ms ( $\Delta t = 2$  μs for the EOD) is used.

### III. RESULTS AND DISCUSSION

Figure 4(a) shows the time-resolved current response of the QLED with TCTA as the hole-transport layer (HTL) under stepwise-increasing voltage. Obviously, the transient current  $i_{tr}$  during the first sweep is larger than that of the



second sweep, as discussed in Fig. 2(c). The current at  $t_0$  and the current difference  $\Delta I$  are shown in Fig. 4(b) as a function of driving voltage. A peak for the current difference is clearly observed, which should be related to the carrier dynamics of the defect states in the semiconductors and will be discussed in the following. In order to identify the origin of traps in devices, single-carrier devices are fabricated and the current and current difference properties are shown in Figs. 4(c) and 4(d). From the current response of the HOD [consisting of TCTA, Fig. 4(c)] and EOD [Fig. 4(d) and Supplemental Material Fig. S4 [39]], we can find that a similar current difference can only be observed in the HOD. Therefore, we conclude that the traps originate from TCTA, rather than from ZnO or QDs.

Meanwhile,  $\Delta I$  curves of the TCTA HOD with different time intervals (between two sequential measurement events) are shown in Fig. 5(a). The  $\Delta I$  increases monotonically with the time interval increasing from 3 to 50 s, then it reaches saturation (identical to that obtained for a fresh device) when a larger interval ( $>60$  s) is used, which is also observed in the TCTA QLED shown in Supplemental Material Fig. S5 [39]. These results demonstrate that the trapping and detrapping processes can recover to the initial states. In other words, the reversible trapping processes are indeed caused by the defects. To further verify this conclusion, the current curves of the TCTA HOD are measured consecutively with an interval of around 300 s,

as shown in Fig. 5(b). The identical current between different measurements indicates that the current difference is indeed induced by a reversible process, rather than material aging caused by water and oxygen, which is often seen as an irreversible phenomenon [12]. Then the transient electroluminescence response (TrEL) of QLEDs with TCTA as the HTL is measured to exclude the effect of hole accumulation on the current difference. As observed from the falling edges shown in Fig. 5(c), the EL intensity drops to zero within 1  $\mu$ s, which means that the lifetime of the holes accumulated in QDs or in the HTL is less than 1  $\mu$ s. In the CPSIV measurement, an inverted biasing process with half period much larger than 1  $\mu$ s is applied to the devices, which ensures that all the accumulated carriers at the interfaces can be depleted before the second sweep. As a result, in the CPSIV measurement, the influence of accumulated carriers on the current difference is eliminated. By inserting a CBP interlayer (5 nm) between TCTA and MoO<sub>3</sub> layers, the injection barrier (0.4 eV) between TCTA and MoO<sub>3</sub> is eliminated and an Ohmic contact is achieved [41], which causes the current to increase by around 2 orders of magnitude, as shown in Supplemental Material Fig. S6 [39]. However, as shown in Fig. 5(d), the current difference is also observed in such an Ohmic contact device, thus excluding the influence of the injection barrier on the current difference. The Joule heating effect in devices during electrical measurements is also evaluated. No discernible

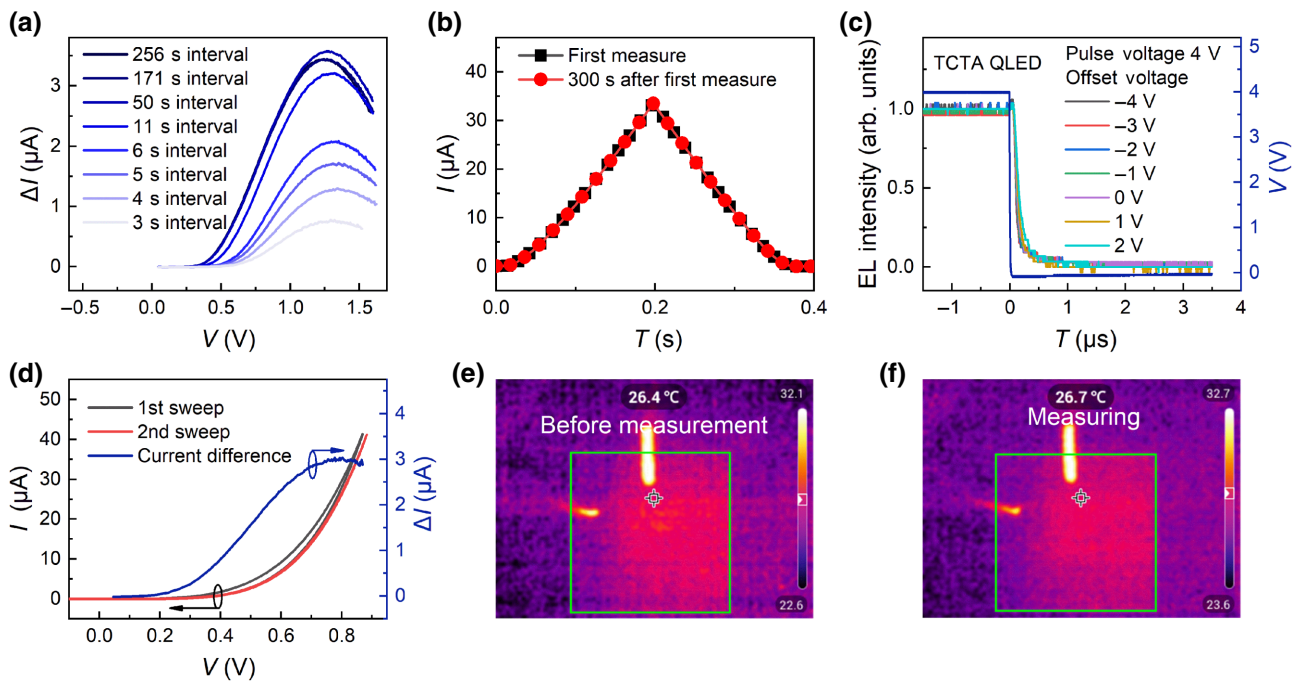


FIG. 5. (a) The current difference of HOD with different time intervals (between two consecutive measurements) from 3 to 256 s. (b) The current curves of TCTA QLEDs measured with around 300 s interval. (c) Falling edges of the TrEL response of TCTA QLED with different offset voltages. (d) The current of the first and second sweeps and the current difference of these two sweeps in the Ohmic contact device with 5-nm CBP as interlayer. The infrared photograph of HOD (e) before and (f) during measurements.

temperature increase is observed during the measurement period (2–3 s) as seen from the infrared photographs of the HOD shown in Figs. 5(e) and 5(f), which excludes the influence of Joule heating effects.

These results provide unambiguous evidence that the charge-carrier trapping and/or capturing processes by the deep traps of TCTA dominate the current difference  $\Delta I$ , which is also confirmed by the trap-filling SCLC curve as shown in the inset of Supplemental Material Fig. S6 [39]. We suspect that the traps in the TCTA films are induced by the electrostatic interaction of water molecules introduced during the fabrication process [45], rather than the water clusters [46,47]. It is noteworthy that, from Fig. 4(d), the traps in the ZnO and QD layers have no effect on the  $\Delta I$ , although defects are reported to widely exist in both ZnO and QDs [17,48]. This should be due to the shallow and short-lifetime nature of these defect traps in ZnO and QDs. In contrast, the long-lifetime properties of these deep traps can be reflected by adjusting the time intervals between two sequential measurements, as shown in Fig. 5(a). A short time interval only allows a few of these trapped holes to be released, which leads to a very small  $\Delta I$ . For the measurements with large time interval, the measured  $\Delta I$  values are identical to each other since these trapped holes are completely released. For the origin of the peak in the  $\Delta I$  curves (Figs. 4 and 5), we think that is caused by the trapping process in the first sweep. The current through the organic films increases with the increase of the driving voltage, which accelerates the charge capturing for the traps, and then reduces the current in the first sweep. As a result, the current difference between the first and the second sweep begins to decrease at a certain driving voltage. Thus, a peak for the current difference is observed, as shown in Fig. 4(b).

Another implication from these results is that the inflection point of the  $\Delta I$  curve means hole injection, from which we can then obtain a key parameter for the EL devices, the hole injection voltage,  $V_{h\text{-inj}}$ . It is well known that the limitation of the turn-on voltage for EL in QLEDs remains an open question. That is, which one determines the EL turn-on of the devices, electron injection or hole injection? According to the previous analysis, the factors limiting the EL turn-on could be distinguished through our proposed measurements. As shown in Fig. 6(a) for the TCTA-based QLED, the  $\Delta I$  curve possesses the same voltage inflection point as the  $L-V$  curve, which implies that the hole injection determines the EL turn-on in QLEDs. This is further confirmed by measuring the  $\Delta I-V$  and  $L-V$  properties of a BCBP-based QLED and the results are shown in Fig. 6(b). The EL turn-on voltage for the QLED is indeed identical to that of  $V_{h\text{-inj}}$  for the  $\Delta I$ . Therefore, we conclude unambiguously that the hole injection means an EL turn-on in the QLEDs, consistent with the recent study Ref. [49]. These results validate the characterization method proposed in this work in characterizing the

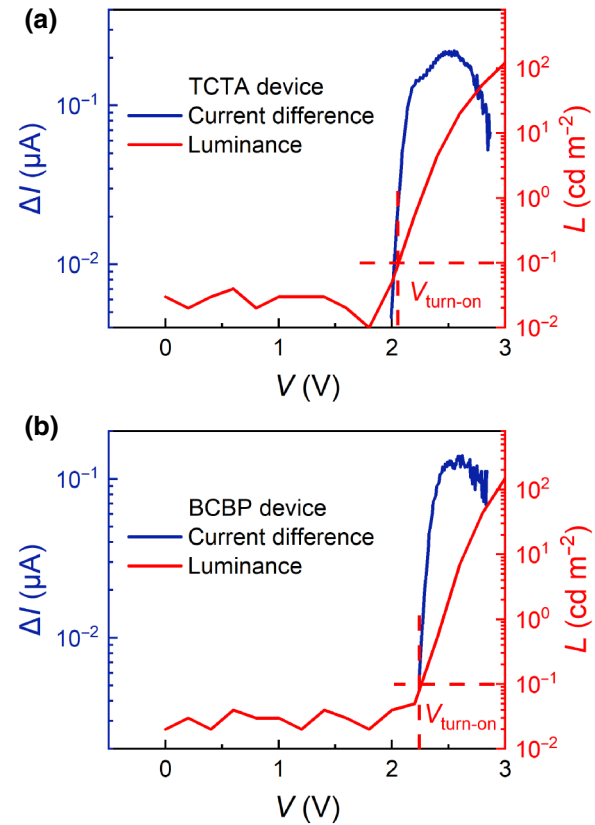


FIG. 6. Current-difference–voltage–luminance curve of QLED with (a) TCTA and (b) BCBP as the hole-injection layers.

working mechanism of QLEDs. We believe there are no technical or fundamental barriers to applying this characterization technology to other LEDs, such as organic LEDs or perovskite LEDs.

Additionally, the influence of deep traps in the HTLs on the device performance is investigated by measuring the photoelectronic properties and operational lifetime of QLEDs based on TCTA and BCBP. In comparison with the TCTA device, the BCBP-based QLED shows smaller leakage current before EL turn-on, which should be due to the stronger electron-blocking ability of BCBP (as discussed in Supplemental Material [39]), which confines the charges to the QD emissive layer, reducing the nonradiative recombination process in the device and thus improving the device efficiency [44]. Meanwhile, the BCBP-based QLED also renders higher current density at higher driving voltages, as observed from Fig. 7(a), which is caused by the lower hole-injection barrier between BCBP and QDs. The lower HOMO energy level of BCBP compared with TCTA (Supplemental Material Fig. S3 [39]) ensures sufficient hole injection into the QDs, leading to the higher device efficiency. As a result, the maximum current efficiency ( $19.9 \text{ cd A}^{-1}$ ) of the BCBP device is larger than that of the TCTA device ( $17.4 \text{ cd A}^{-1}$ ), as shown in

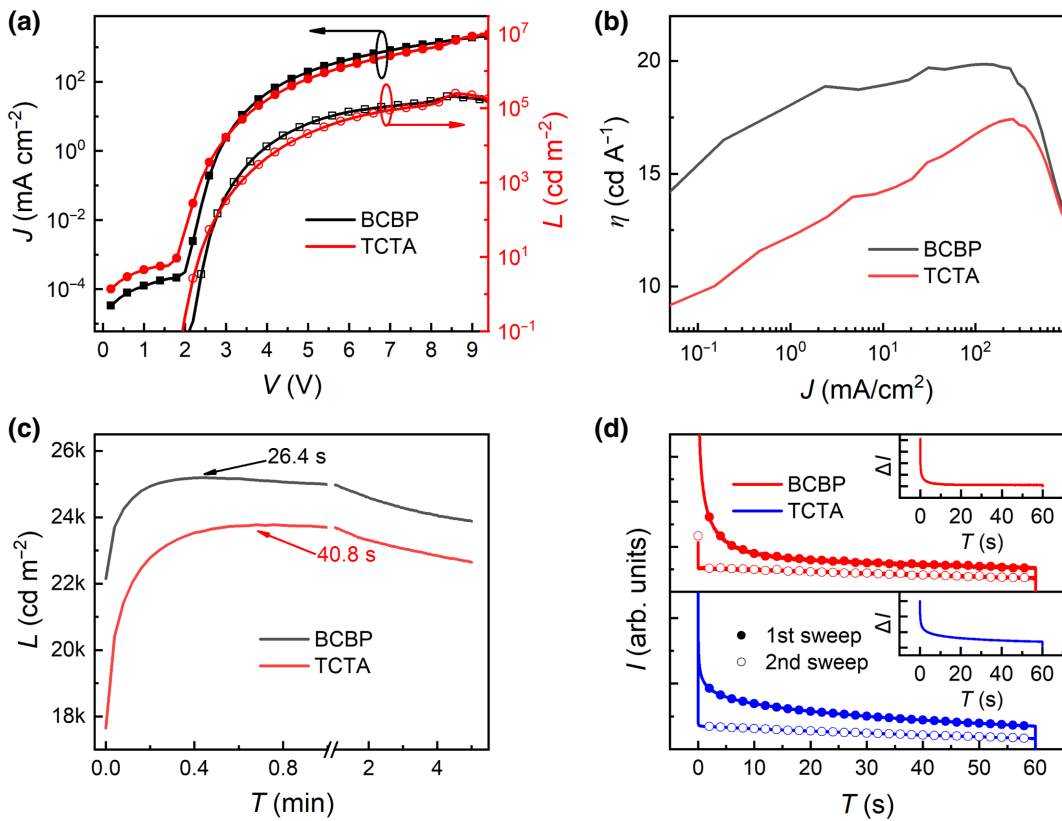


FIG. 7. The characteristics of QLEDs with 60-nm BCBP and 60-nm TCTA. (a) Current density–voltage–luminance. (b) Current efficiency–current density. (c) The luminance–time curve under  $5 \text{ mA cm}^{-2}$ . (d) The transient current–time curves of HODs with 150-nm BCBP and 150-nm TCTA under continuous pulse voltage (high voltage 10 V lasts for 60 s, low voltage 0 V lasts 10 ms). The insets show the corresponding current differences of these two devices between the two driving voltage pulses.

Fig. 7(b). Figure 7(c) shows the operational lifetime properties of both TCTA and BCBP devices driven under  $5 \text{ mA cm}^{-2}$ . It can be seen that both of these devices exhibit a luminance overshoot at the initial stage. The duration for this overshoot is around 41 and 26 s for TCTA- and BCBP-based devices, respectively. Considering the similar device structure of these two QLEDs, we deduce that the different luminance overshoots should originate from different defect traps in TCTA and BCBP. Then, the current responses of the HOD with BCBP or TCTA driven by two continuous voltage pulses are measured and the results are shown in Fig. 7(d). We can find that there is a slow current drop during the first voltage pulse for both TCTA and BCBP devices, which is not observed during the second voltage pulse. These are identical to the discussion depicted in Fig. 2(c), which is attributed to the deep trapping effect. However, the drop time is very different for these two devices; it is longer for the TCTA-based HOD. The current differences between the two driving voltage pulses are plotted in the insets in Fig. 7(d), and it is clear that the drop time (i.e., trap-filling process) in the TCTA and BCBP layer is around 45 and 20 s, respectively, which is consistent with the time of luminance overshoot of these

two QLEDs. Therefore, we can give a conclusion that the luminance overshoot during the lifetime measurement is induced by the deep hole traps in HTLs.

#### IV. CONCLUSION

In summary, we propose a low-cost characterization method referred to as CPSIV, which is a facile and reliable technology to characterize the long-lived traps in hole transport layers. With the commonly used hole-transport material TCTA as the model HTL, the validity of this characterization technology is confirmed. The detrapping time is on the order of seconds. This *in situ* measurement is used to explore the working mechanisms of QLEDs. Through CPSIV measurements, it is clarified that the EL turn-on in the QLEDs is determined by the hole injection rather than electron injection. We believe that there are no obstacles to extending our proposed CPSIV technology to the probing of long-lived traps in other semiconductor materials, such as polymers and metal halide perovskites, as well as photoelectronic devices consisting of these materials. It is notable that this CPSIV cannot work in a device consisting

of trap-free films, which will lead to the current difference of approximately 0 between different sweeps.

## ACKNOWLEDGMENTS

We acknowledge support from the National Natural Science Foundation of China (Grants No. 12274173, No. 11974141, and No. 12074148).

- [1] C. Xiang, L. Wu, Z. Lu, M. Li, Y. Wen, Y. Yang, W. Liu, T. Zhang, W. Cao, S. W. Tsang, B. Shan, X. Yan, and L. Qian, High efficiency and stability of ink-jet printed quantum dot light emitting diodes, *Nat. Commun.* **11**, 1646 (2020).
- [2] Q. Yuan, T. Wang, P. Yu, H. Zhang, H. Zhang, and W. Ji, A review on the electroluminescence properties of quantum-dot light-emitting diodes, *Org. Electron.* **90**, 106086 (2021).
- [3] H. Shen, Q. Gao, Y. Zhang, Y. Lin, Q. Lin, Z. Li, L. Chen, Z. Zeng, X. Li, Y. Jia, S. Wang, Z. Du, L. S. Li, and Z. Zhang, Visible quantum dot light-emitting diodes with simultaneous high brightness and efficiency, *Nat. Photonics* **13**, 192 (2019).
- [4] X. Dai, Z. Zhang, Y. Jin, Y. Niu, H. Cao, X. Liang, L. Chen, J. Wang, and X. Peng, Solution-processed, high-performance light-emitting diodes based on quantum dots, *Nature* **515**, 96 (2014).
- [5] J. Song, O. Wang, H. Shen, Q. Lin, Z. Li, L. Wang, X. Zhang, and L. S. Li, Over 30% external quantum efficiency light-emitting diodes by engineering quantum dot-assisted energy level match for hole transport layer, *Adv. Funct. Mater.* **29**, 1808377 (2019).
- [6] H. J. Jang, J. Y. Lee, G. W. Baek, J. Kwak, and J.-H. Park, Progress in the development of the display performance of AR, VR, QLED and OLED devices in recent years, *J. Inf. Disp.* **23**, 1 (2022).
- [7] H. Luo, W. Zhang, M. Li, Y. Yang, M. Guo, S. W. Tsang, and S. Chen, Origin of subthreshold turn-on in quantum-dot light-emitting diodes, *ACS Nano* **13**, 8229 (2019).
- [8] L. Qian, Y. Zheng, K. R. Choudhury, D. Bera, F. So, J. Xue, and P. H. Holloway, Electroluminescence from light-emitting polymer/ZnO nanoparticle heterojunctions at sub-bandgap voltages, *Nano Today* **5**, 384 (2010).
- [9] D. Chen, D. Chen, X. Dai, Z. Zhang, J. Lin, Y. Deng, Y. Hao, C. Zhang, H. Zhu, F. Gao, and Y. Jin, Shelf-stable quantum-dot light-emitting diodes with high operational performance, *Adv. Mater.* **32**, 2006178 (2020).
- [10] Z. Chen, Q. Su, Z. Qin, and S. Chen, Effect and mechanism of encapsulation on aging characteristics of quantum-dot light-emitting diodes, *Nano Res.* **14**, 320 (2020).
- [11] S. Chen, W. Cao, T. Liu, S. W. Tsang, Y. Yang, X. Yan, and L. Qian, On the degradation mechanisms of quantum-dot light-emitting diodes, *Nat. Commun.* **10**, 765 (2019).
- [12] J. H. Chang, P. Park, H. Jung, B. G. Jeong, D. Hahm, G. Nagamine, J. Ko, J. Cho, L. A. Padilha, D. C. Lee, C. Lee, K. Char, and W. K. Bae, Unraveling the origin of operational instability of quantum dot based light-emitting diodes, *ACS Nano* **12**, 10231 (2018).
- [13] H. F. Haneef, A. M. Zeidell, and O. D. Jurchescu, Charge carrier traps in organic semiconductors: A review on the underlying physics and impact on electronic devices, *J. Mater. Chem. C* **8**, 759 (2020).
- [14] X. Qiu, Y. Liu, W. Li, and Y. Hu, Traps in metal halide perovskites: Characterization and passivation, *Nanoscale* **12**, 22425 (2020).
- [15] S. Kahmann and M. A. Loi, Trap states in lead chalcogenide colloidal quantum dots-origin, impact, and remedies, *Appl. Phys. Rev.* **7**, 041305 (2020).
- [16] R. Ye, X. Cai, C. Du, H. Liu, Y. Zhang, X. Duan, and J. Zhu, An overview on analyses and suppression methods of trapping effects in AlGaN/GaN HEMTs, *IEEE Access* **10**, 21759 (2022).
- [17] J. Wang and N. C. Greenham, Charge transport in colloidal ZnO nanocrystal solids: The significance of surface states, *Appl. Phys. Lett.* **104**, 193111 (2014).
- [18] Y. Wang, X. Zhu, X. Xue, X. Chi, R. Wang, and W. Ji, Electron transport mechanism in colloidal SnO<sub>2</sub> nanoparticle films and its implications for quantum-dot light-emitting diodes, *J. Phys. D: Appl. Phys.* **55**, 374004 (2022).
- [19] T. Ogawa, T. Kuzuya, Y. Hamanaka, and K. Sumiyama, Synthesis of Ag-In binary sulfide nanoparticles-structural tuning and their photoluminescence properties, *J. Mater. Chem.* **20**, 2226 (2010).
- [20] L. Li, A. Pandey, D. J. Werder, B. P. Khanal, J. M. Pietryga, and V. I. Klimov, Efficient synthesis of highly luminescent copper indium sulfide-based core/shell nanocrystals with surprisingly long-lived emission, *J. Am. Chem. Soc.* **133**, 1176 (2011).
- [21] C. Li, L. Duan, H. Li, and Y. Qiu, Universal trap effect in carrier transport of disordered organic semiconductors: Transition from shallow trapping to deep trapping, *J. Phys. Chem. C* **118**, 10651 (2014).
- [22] H. Li, C. Li, L. Duan, and Y. Qiu, Charge transport in amorphous organic semiconductors: Effects of disorder, carrier density, traps, and scatters, *Isr. J. Chem.* **54**, 918 (2014).
- [23] C. Li, L. Duan, Y. Sun, H. Li, and Y. Qiu, Charge transport in mixed organic disorder semiconductors: Trapping, scattering, and effective energetic disorder, *J. Phys. Chem. C* **116**, 19748 (2012).
- [24] R. Wang, Y. T. Zhang, and J. Q. Yao, Abnormal temperature dependence of mobility in a disordered system with traps: Experiment and theory, *IEEE Photonics J.* **7**, 1 (2015).
- [25] J. Tang, F. Li, G. Yang, Y. Ge, Z. Li, Z. Xia, H. Shen, and H. Zhong, Reducing the chromaticity shifts of light-emitting diodes using gradient-alloyed Cd<sub>x</sub>Zn<sub>1-x</sub>Se<sub>y</sub>S<sub>1-y</sub>@ZnS core shell quantum dots with enhanced high-temperature photoluminescence, *Adv. Opt. Mater.* **7**, 1801687 (2019).
- [26] R. Cai, X. Qu, H. Liu, H. Yang, K. Wang, and X. W. Sun, Perovskite light-emitting diodes based on FAPbI<sub>1-x</sub>Sn<sub>x</sub>Br<sub>3</sub> nanocrystals synthesized at room temperature, *IEEE Trans. Nanotechnol.* **18**, 1050 (2019).
- [27] V. Kumar, S. C. Jain, A. K. Kapoor, J. Poortmans, and R. Mertens, Trap density in conducting organic semiconductors determined from temperature dependence of *J-V* characteristics, *J. Appl. Phys.* **94**, 1283 (2003).
- [28] I. Solomon, R. Benferhat, and H. T. Quoc, Space-charge-limited conduction for the determination of the midgap density of states in amorphous silicon: Theory and experiment, *Phys. Rev. B* **30**, 3422 (1984).
- [29] J. M. Montero and J. Bisquert, Interpretation of trap-limited mobility in space-charge limited current in organic layers

- with exponential density of traps, *J. Appl. Phys.* **110**, 043705 (2011).
- [30] S. Nešpůrek and J. Sworakowski, Spectroscopy of local states in molecular materials using space-charge-limited currents, *Int. J. Radiat. Appl. Instrum. Part C* **36**, 3 (1990).
- [31] P. Mark and W. Helffrich, Space-charge-limited currents in organic crystals, *J. Appl. Phys.* **33**, 205 (1962).
- [32] L. Xu, J. Wang, and J. W. P. Hsu, Transport Effects on Capacitance-Frequency Analysis for Defect Characterization in Organic Photovoltaic Devices, *Phys. Rev. Appl.* **6**, 064020 (2016).
- [33] P. P. Boix, G. Garcia-Belmonte, U. Muñecas, M. Neophytou, C. Waldauf, and R. Pachos, Determination of gap defect states in organic bulk heterojunction solar cells from capacitance measurements, *Appl. Phys. Lett.* **95**, 233302 (2009).
- [34] J. A. Carr, M. Elshobaki, and S. Chaudhary, Deep defects and the attempt to escape frequency in organic photovoltaic materials, *Appl. Phys. Lett.* **107**, 203302 (2015).
- [35] D. Bozyigit, S. Volk, O. Yarema, and V. Wood, Quantification of deep traps in nanocrystal solids, their electronic properties, and their influence on device behavior, *Nano Lett.* **13**, 5284 (2013).
- [36] D. Bozyigit, M. Jakob, O. Yarema, and V. Wood, Deep level transient spectroscopy (DLTS) on colloidal-synthesized nanocrystal solids, *ACS Appl. Mater. Interfaces* **5**, 2915 (2013).
- [37] D. V. Lang, Deep-level transient spectroscopy: A new method to characterize traps in semiconductors, *J. Appl. Phys.* **45**, 3023 (1974).
- [38] Y. Tanaka, Y. Noguchi, M. Kraus, W. Brüttig, and H. Ishii, Displacement current measurement of a pentacene metal-insulator-semiconductor device to investigate both quasi-static and dynamic carrier behavior using a combined waveform, *Org. Electron.* **12**, 1560 (2011).
- [39] See Supplemental Material at <http://link.aps.org/supplemental/10.1103/PhysRevApplied.19.024010> for further experimental results and analysis, details on materials, device fabrication, and characterization.
- [40] Y. Noguchi, H. Ishii, T. Tamura, and H. J. Kim, Device properties of Alq<sub>3</sub>-based organic light-emitting diodes studied by displacement current measurement, *J. Photonics Energy* **2**, 021214 (2012).
- [41] N. B. Kotadiya, H. Lu, A. Mondal, Y. Ie, D. Andrienko, P. W. M. Blom, and G. A. H. Wetzelaer, Universal strategy for Ohmic hole injection into organic semiconductors with high ionization energies, *Nat. Mater.* **17**, 329 (2018).
- [42] W. Ji, P. Jing, L. Zhang, D. Li, Q. Zeng, S. Qu, and J. Zhao, The work mechanism and sub-bandgap-voltage electroluminescence in inverted quantum dot light-emitting diodes, *Sci. Rep.* **4**, 6974 (2014).
- [43] C. Zang, M. Xu, L. Zhang, S. Liu, and W. Xie, Organic–inorganic hybrid thin film light-emitting devices: Interfacial engineering and device physics, *J. Mater. Chem. C* **9**, 1484 (2021).
- [44] S. Rhee, J. H. Chang, D. Hahm, B. G. Jeong, J. Kim, H. Lee, J. Lim, E. Hwang, J. Kwak, and W. K. Bae, Tailoring the electronic landscape of quantum dot light-emitting diodes for high brightness and stable operation, *ACS Nano* **14**, 17496 (2020).
- [45] G. Zuo, M. Linares, T. Upreti, and M. Kemerink, General rule for the energy of water-induced traps in organic semiconductors, *Nat. Mater.* **18**, 588 (2019).
- [46] N. B. Kotadiya, A. Mondal, S. Xiong, P. W. M. Blom, D. Andrienko, and G. J. A. H. Wetzelaer, Rigorous characterization and predictive modeling of hole transport in amorphous organic semiconductors, *Adv. Electron. Mater.* **4**, 1800366 (2018).
- [47] N. B. Kotadiya, A. Mondal, P. W. M. Blom, D. Andrienko, and G. A. H. Wetzelaer, A window to trap-free charge transport in organic semiconducting thin films, *Nat. Mater.* **18**, 1182 (2019).
- [48] D. S. Ginger and N. C. Greenham, Charge injection and transport in films of CdSe nanocrystals, *J. Appl. Phys.* **87**, 1361 (2000).
- [49] Q. Su and S. Chen, Thermal assisted up-conversion electroluminescence in quantum dot light emitting diodes, *Nat. Commun.* **13**, 369 (2022).